Influence of Cis and Trans Ligands in Platinum(II) Complexes on the Ability of the Platinum Center to Activate C−H Bonds. A Density Functional Theory Study

Hongjuan Zhu and Tom Ziegler*

Department of Chemistry, University of Calgary, 2500 University Drive, N.W. Calgary, Alberta, Canada T2N 1N4

Received November 14, 2007

We have studied the influence of different ligands X (X = F, Cl, Br, I, NO_2, and CN) on the C−H bond activation of CH_4 in *trans*-$PtCl_2X(CH_4)^-$, **1**, and *trans*-$PtClX_2(CH_4)^-$, **2**, where X is either trans (**1**) or cis (**2**) to methane. For **1** with X in the trans position, the *trans*-$PtCl_2X^-$ fragment interacts with CH_4 through the overlap between the empty d_σ-based orbital $2a_1$ pointing along the Pt−X direction and σ_{CH} on CH_4. An interaction also takes place between an occupied d_σ-based orbital $1b_1$ and the empty σ^*_{CH} orbital on CH_4, where the d_π metal orbital is positioned perpendicular to the $PtCl_2X^-$ plane. The d_σ metal orbital contribution in $2a_1$ is antibonding with respect to σ_x on X, whereas d_π in $1b_1$ is antibonding with respect to π_x. Through the series F, Cl, Br, I, NO_2, and CN, the energies of σ_x and π_x increase. This is mostly an electronegativity effect. The increase in energy causes an increase in the contribution from σ_x and π_x to $2a_1$ and $1b_1$, respectively. As a consequence, the bonding overlaps $\langle\sigma_{CH}|2a_1\rangle$ and $\langle\sigma^*_{CH}|1b_1\rangle$ will diminish, as only the d-component in $2a_1$ and $1b_1$ contributes to the overlap. As a result of the decreasing bonding overlaps, the Pt−CH_4 bond strength will decline. It is thus shown that the experimentally established order of trans-labilizing power for the series of ligands X studied here, F < Cl < Br < I < NO_2 < CN, can be related to the orbital energies of σ_x and π_x and the electronegativity of the elements that are involved in these orbitals. The labilization of the Pt−CH_4 bond in the C−H activation transition state is even larger than in the adduct **1**, leading to an increase in the C−H activation barrier along the series F < Cl < Br < I < NO_2 < CN. For **2** with X in the cis position, solvation has the largest influence on trends in the Pt−CH_4 bond for both **2** and the transition state. However C−H activation barriers are quite similar for different X.

1. Introduction

In the Shilov reaction,[1,2] methane replaces H_2O in *cis*-$PtCl_2(H_2O)_2$ to form *cis*-$PtCl_2(H_2O)(CH_4)$ followed by C−H activation. We have found in a recent theoretical study[3] that the rate-determining step of methane activation by $PtCl_2(H_2O)_2$ is the uptake of CH_4 via an associative S_N2 substitution reaction rather than the C−H activation step. Shteinman et al.[4] have extended the scope of the original Shilov reaction to involve the activation of methane by *cis*-$PtX_2(H_2O)_2$ with X = F, Cl, Br, I, NO_2, and CN. We find in a theoretical analysis[5] of the Shteinman experiment that the uptake of CH_4 to form *cis*-$PtX_2(H_2O)(CH_4)$ rather than C−H activation again is rate-determining for methane activation, independent of X. It was however found that the barrier of C−H activation in *cis*-$PtX_2(H_2O)(CH_4)$ increases through the series F < Cl < Br < I < NO_2 < CN. We shall in the current investigation examine in more detail how the different ligand, X, influences the C−H activation barrier when placed either cis or trans to methane. Our analysis will be based on a bond energy decomposition scheme that takes into account both steric and electron interactions between CH_4 and the platinum center with its co-ligands including X. A similar bond decomposition analysis will be performed to understand how X influences the barrier in the S_N2 substitution reaction that replaces H_2O with CH_4. As an outcome of this bond decomposition analysis, we shall provide new insight into the factors that make X a strong or weak trans-directing ligand in the ground state as well as the transition state.

2. Computational Details

Results were obtained from DFT calculations based on the Becke−Perdew exchange−correlation functional,[6–8] using the Amsterdam Density Functional (ADF) program.[9] A standard double-ζ STO basis with one set of polarization functions was applied for the H, N, F, Cl, Br, C, and O atoms, while a standard triple-ζ basis set was employed for the I and Pt atoms. The 1s electrons of N, C, F, and O, as well as the 1s−2p electrons of Cl, 1s−3d electrons of Br, 1s−4d electrons of I, and 1s−4f electrons of Pt, were treated as a frozen core. A standard set of auxiliary s, p, d, f, and g STO functions, centered on each

* Corresponding author. E-mail: ziegler@ucalgary.ca.

(1) Gol'dshleger, N. F.; Tyabin, M. B.; Shilov, A. E.; Shteinman, A. A. *Zh. Fiz. Khim. (Engl. Transl.)* **1969**, *43*, 1222.
(2) Gol'dshleger, N. F.; Es'kova, V. V.; Shilov, A. E.; Shteinman, A. A. *Zh. Fiz. Khim. (Engl. Transl.)* **1972**, *46*, 785.
(3) Zhu, H.; Ziegler, T. *J. Organomet. Chem.* **2006**, *691*, 4486.
(4) Gol'dshleger, N. F.; Shteinman, A. A. *React. Kinet. Catal. Lett.* **1977**, *6*, 43.
(5) Zhu, H.; Ziegler, T. *Organometallics* **2007**, *26*, 2277.
(6) Becke, A. *Phys. Rev. A* **1988**, *38*, 3098.
(7) Perdew, J. P. *Phys. Rev. B* **1986**, *34*, 7406.
(8) Perdew, J. P. *Phys. Rev. B* **1986**, *33*, 8822.
(9) Te Velde, G.; Bickelhaupt, F. M.; Baerends, E. J.; van Gisbergen, S.; Guerra, C. F.; Snijders, J. G.; Ziegler, T. *J. Comput. Chem.* **2001**, *22*, 931.

10.1021/om701149f CCC: $40.75
Publication on Web 03/29/2008

nucleus, was used to fit the electron density and calculate the Coulomb and exchange potentials in each SCF cycle. The reported energies include first-order scalar relativistic corrections.[10] Gas-phase electronic enthalpies were calculated from the Kohn–Sham energies. For all free energy values reported, the electronic entropy was neglected and standard expressions[11] were used to calculate the remaining gas-phase enthalpic and entropic contributions at nonzero temperature, as well as the zero-point vibrational contribution.

Thermodynamic parameters for the solvation of the halogen ions were obtained from a recent compilation of experimental values.[12] The remaining solvation enthalpies were obtained using the COSMO method[13] as implemented in ADF.[14] The solvent excluding surface was used along with an epsilon value of 78.5 for the dielectric constant of water as the solvent. Atomic radii employed were 1.39, 1.8, 1.16, 1.4, 1.3, 2.3, 1.96, 1.33, and 2.2 Å for Pt, Cl, H, N, O, C, Br, F, and I, respectively. Although the Born energy reported by the COSMO model is, strictly speaking, a free energy, the entropic contribution amounts to perhaps 2% of the total energy.[15] The solvation enthalpy was therefore taken as the difference between the gas-phase energy and that calculated using the COSMO solvation model.

For the purpose of calculating the remaining solvation entropies, the solvation process was broken up into three steps, following Wertz.[16] Here, the solute in the gas phase is first compressed to the molar volume of the solvent. The compressed solute gas then loses the same fraction of its entropy as would be lost by the solvent in going from gas (at its liquid-phase density) to liquid. Finally, the solute gas is extended to the concentration of the desired solution (i.e., 1.0 mol/L).

The solute entropy change for the first and third steps, which are strictly changes in molar volume, is given by $\Delta S = R\mathrm{In}(V_{m,f}/V_{m,i})$, where $V_{m,f}$ is the final solute molar volume and $V_{m,i}$ is the intial solute value. The entropy fraction α lost in the second step can be determined from the absolute entropies of the solvent in its gas ($S_{gas}°$) and liquid ($S_{liq}°$) phases, as shown in eq 1.

$$\alpha = \frac{S^{o}(S^{o} + R\mathrm{In}V_{m,liq}/V_{m,gas})}{(S^{o} + R\mathrm{In}V_{m,liq}/V_{m,gas})} \quad (1)$$

Substituting the appropriate parameters for water[17] affords the value of $\alpha = -0.46$. The sum of the entropy changes accompanying each of the three steps then gives the total solvation entropy; at a temperature of 298.15 K, we have (again, for water) eq 2.

$$\Delta S_{sol} = (-14.3\mathrm{cal{\cdot}mol^{-1}{\cdot}K^{-1}}) - 0.46(S_{gas} - 14.3\mathrm{cal{\cdot}mol^{-1}{\cdot}K^{-1}}) + (7.98\mathrm{cal{\cdot}mol^{-1}{\cdot}K^{-1}}) \quad (2)$$

It is convenient that (by chance) the constant terms independent of $S°$ in eq 2 nearly cancel on expansion, and the solvation entropy in water can therefore be approximated in more qualitative discussions as 50% of the gas-phase entropy $S_{gas}°$, with the opposite sign.

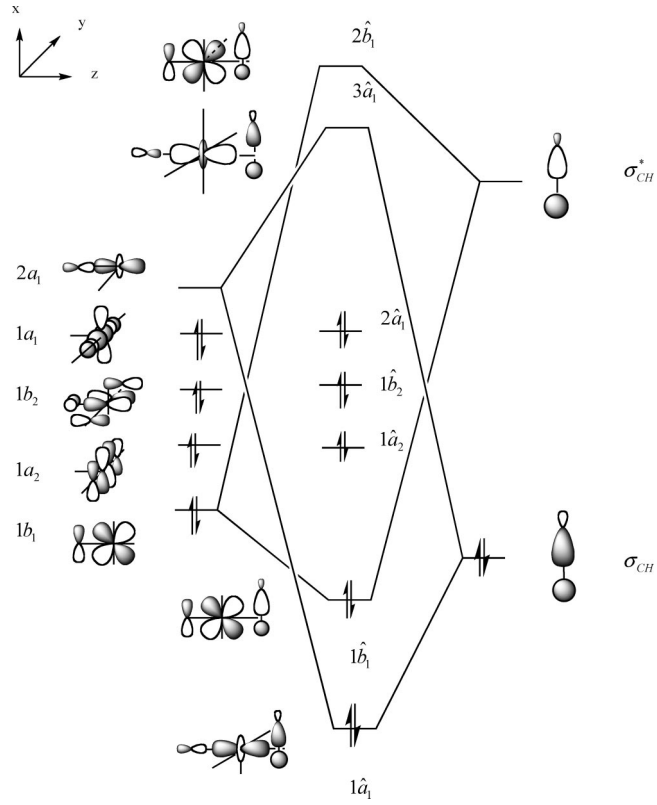

Figure 1. Orbital diagram of the formation of *trans*-$PtCl_2X(CH_4)^-$ from *trans*-$PtCl_2X^-$ and CH_4 fragments.

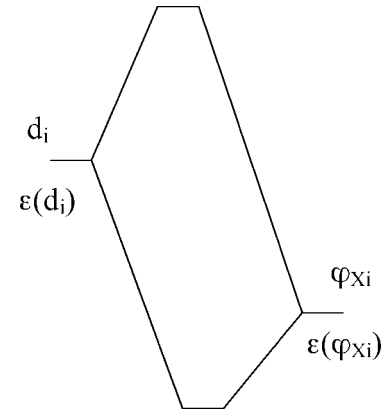

Figure 2. Orbital interaction between d_i metal orbital and φ_{Xi} ligand orbital.

3. Results and Discussion

We shall now study the influence of the ligand X on the strength of the Pt−CH_4 bond in *trans*-$PtCl_2X(CH_4)^-$ when methane is trans to X as well as *trans*-$PtX_2Cl(CH_4)^-$ when CH_4 is cis to X. Our analysis will consider the orbital interaction between *trans*-$PtCl_2X^-$ and CH_4 in the trans case and the interaction between *trans*-PtX_2Cl^- and CH_4 in the cis case. We shall begin with the interaction between *trans*-$PtCl_2X^-$ and CH_4. To this end, we need first to analyze the frontier orbitals of *trans*-$PtCl_2X^-$.

3.1. Orbital Interaction in *trans*-$PtCl_2X^-$. Figure 1 illustrates the orbital interaction diagram between the *trans*-$PtCl_2X^-$ and CH_4 fragments. On the left-hand side, we display

(10) Ziegler, T.; Tschinke, V.; Baerends, E. J.; Snijders, J. G.; Ravenek, W. *J. Phys. Chem.* **1989**, *93*, 3050.
(11) McQuarrie, D. A. *Statistical Thermodynamics*; Harper: New York, 1973.
(12) Fawcett, W. R. *J. Phys. Chem. B* **1999**, *103*, 11181.
(13) Klamt, A.; Schuurmann, G. *J. Chem. Soc., Perkin. Trans. 2* **1993**, 799.
(14) Pye, C. C.; Ziegler, T. *Theor. Chem. Acc.* **1999**, *101*, 396.
(15) Dasent, W. E. *Inorganic Energetics*; Penguin: Middlesex, U.K., 1970.
(16) Wertz, D. H. *J. Am. Chem. Soc.* **1980**, *102*, 5316.
(17) Lide, D. R. *CRC Handbook of Chemistry and Physics*, 76th ed.; CRC Press: New York, 1995.

Table 1. Percent Contribution[a] from Ligand Combinations to the Frontier Orbitals of *trans*-$PtCl_2X^-$

	percent contribution from φ_{Xi}	
ligand X	$2a_1(d_{z^2})^b$	$1b_1(d_{xz})^c$
F	31.4	20.8
Cl	40.1	29.5
Br	42.6	32.4
I	47.7	34.5
NO_2	45.5	31.4
CN	48.3	35.5

[a] $C_i^2 \times 10^2$ where C_i is defined in eq 4. [b] Percent contribution from σ_x to the $2a_1$ orbital of *trans*-$PtCl_2X^-$. [c] Percent contribution from π_x to $1b_1$ of *trans*-$PtCl_2X^-$.

Table 2. Energies[a] of $\epsilon(\varphi^{\sigma}_{Xi})$ and $\epsilon(\varphi^{\pi}_{Xi})$ for Different Ligands X (X = F, Cl, Br, I, NO_2, and CN)

X^b	$\epsilon(\varphi^{\sigma}_{Xi})$	$\epsilon(\varphi^{\pi}_{Xi})$
F	−30.309	−11.523
Cl	−21.047	−8.809
Br	−20.381	−8.000
I	−17.689	−7.171
NO_2	−16.920	−6.397
CN	−12.217	−9.421

[a] ϵ in eV. [b] Orbital energies of neutral ligands.

a simplified orbital diagram for the *trans*-$PtCl_2X^-$ fragment, containing the five antibonding d-based frontier orbitals. The LUMO is an antibonding combination between d_{z^2} and the trans σ_x orbital on X, whereas the HOMO is an out-of-phase combination between $d_{x^2-y^2}$ and two cis σ_{Cl} orbitals on the two chlorines. We have in addition three dπ orbitals destabilized by antibonding interactions with π-ligand orbitals. The interaction of the Pt orbital and the ligand combination can be explained by perturbation theory (see Figure 2).

The upper valence levels in Figure 2 are represented by d orbitals destabilized by out-of-phase antibonding interactions with the ligands. We can write the destabilized d orbitals as

$$\Psi_i = d_i - C_i\varphi_{Xi} (i = 1, 5) \tag{3}$$

where φ_{Xi} is the ligand orbital combination that interacts with d_i. We have from perturbation theory that C_i of eq 3 is given by

$$C_i = \frac{\langle d_i|H|\varphi_{Xi}\rangle}{\epsilon(d_i) - \epsilon(\varphi_{Xi})} \tag{4}$$

where $\epsilon(d_i)$ and $\epsilon(\varphi_{Xi})$ are the orbital energies of d_i and φ_{Xi}, respectively, as shown in Figure 2. It is clear that the larger the C_i in absolute terms, the larger the percent contribution of φ_{Xi} to Ψ_i. We present in Table 1 $C_i^2 \times 10^2$ for $2a_1$ and $1b_1$ of Figure 1 for different X. It follows for both the d_{z^2}-based LUMO and the d_{xz}-based HOMO−3 that the percent contribution from φ_{Xi} to these orbitals with different trans ligands X follows the order F < Cl < Br < I < NO_2 < CN.

An analysis of the trend in Table 1 shows that it is set primarily by $\epsilon(\varphi_{Xi})$ in the denominator for the expression for C_i in eq 4. Thus, the more electronegative the ligand X is, the larger $-\epsilon(\varphi_{Xi})$ will be, Table 2, and the smaller the C_i^2 percent contribution from φ_{Xi}.

3.2. Orbital Interaction in $PtCl_2X(CH_4)^-$. Having analyzed the frontier orbitals of $PtCl_2X^-$, we now turn toward the interaction between $PtCl_2X^-$ and methane to form the methane adduct $PtCl_2X(CH_4)^-$. It can see from Figure 1 that the interaction diagram for the formation of $PtCl_2X(CH_4)^-$ involves the occupied σ_{CH} orbital of CH_4 and the LUMO $2a_1$ of $PtCl_2X^-$

Table 3. Composition[a,b] of the Bonding Orbitals $1\hat{a}_1$ and $1\hat{b}_1$ of $PtCl_2X(CH_4)^-$ in Terms of CH_4 and $PtCl_2X^-$ Fragment Contributions

	composition	
ligand	$C_2^2 \times 10^2$ in $1\hat{a}_1$	$C_3^2 \times 10^2$ in $1\hat{b}_1$
F	4.3	6.2
Cl	4.2	4.3
Br	4.0	3.7
I	4.0	1.4
NO_2	2.6	1.0
CN	2.2	0

[a] C_2 is defined in eq 6 as the contribution to $1\hat{a}_1$ from $\psi(2a_1)$. [b] C_3 is defined in eq 8 as the contribution from σ^*_{CH} to $1\hat{b}_1$.

Table 4. Bonding Overlaps in $1\hat{a}_1$ and $1\hat{b}_1$ of $PtCl_2X(CH_4)^-$ between CH_4 and $PtCl_2X^-$ Fragment Orbitals

	overlap	
ligands	$\langle\sigma_{CH}\|\psi(2a_1)\rangle$ [a]	$\langle\sigma^*_{CH}\|\psi(1b_1)\rangle$ [b]
F	3.17×10^{-1}	1.69×10^{-1}
Cl	2.29×10^{-1}	1.54×10^{-1}
Br	2.25×10^{-1}	1.49×10^{-1}
I	2.17×10^{-1}	1.46×10^{-1}
NO_2	1.80×10^{-1}	1.30×10^{-1}
CN	1.56×10^{-1}	0.78×10^{-1}

[a] Bonding overlap in $1\hat{a}_1$. [b] Bonding overlap in $1\hat{b}_1$.

leading to the bonding orbital $1\hat{a}_1$ as well as the empty σ^*_{CH} of CH_4 and the occupied $1b_1$ orbital of $PtCl_2X^-$ leading to the bonding orbital $1\hat{b}_1$. We can write

$$\psi(1\hat{a}_1) = \sigma_{CH} + C_2\psi(2a_1) \tag{5}$$

where

$$C_2 = \frac{\langle\sigma_{CH}|H|\psi(2a_1)\rangle}{\epsilon(2a_1) - \epsilon(\sigma_{CH})} \tag{6}$$

and

$$\psi(1\hat{b}_1) = \psi(1b_1) + C_3\sigma^*_{CH} \tag{7}$$

with

$$C_3 = \frac{\langle\sigma^*_{CH}|H|\psi(1b_1)\rangle}{\epsilon(\sigma^*_{CH}) - \epsilon(1b_1)} \tag{8}$$

We display in Table 3 the contributions from $\psi(2a_1)$ to $\psi(1\hat{a}_1)$ and from σ^*_{CH} to $\psi(1\hat{b}_1)$ for different trans ligands X. We find in both cases the order F > Cl > Br > I > NO_2 > CN. This trend correlates with the corresponding order for the overlaps $\langle\sigma_{CH}|\psi(2a_1)\rangle$ and $\langle\sigma^*_{CH}|\psi(1b_1)\rangle$ given by F > Cl > Br > I > NO_2 > CN as shown in Table 4.

The trend in the overlaps is in turn a consequence of the d orbital participation in $\psi(1b_1)$ and $\psi(2a_1)$. The more electronegative the X ligand, the larger the d participation in $\psi(1b_1)$ and $\psi(2a_1)$, and the larger the interacting overlaps of $\langle\sigma_{CH}|\psi(2a_1)\rangle$ and $\langle\sigma^*_{CH}|\psi(1b_1)\rangle$.

For square-planar platinum complexes *trans*-$PtXCl_2L^-$, it is well established experimentally that the ability of X to destabilize the Pt−L bond trans to it follows the order[18] F < Cl < Br < I < NO_2 < CN. It seems that the order of this "trans influence"[19] at the most fundamental level is related to the electronegativity of X, according to our analysis in Sections

(18) Harrley, F. R. *Chem. Soc. Rev.* **1973**, *2*, 163.
(19) Pidcock, A. *J. Chem. Soc., A* **1966**, 1707.

Table 5. Decomposition of the Bonding Energy[a,d] between the *trans*-$PtCl_2X^-$ Fragment and the CH_4 Fragment in *trans*-$PtCl_2X(CH_4)^-$ for Different X (X = F, Cl, Br, I, NO_2, and CN)

X	ΔE_{dist}	ΔE^c_{steric}	$\Delta E_{orbital}$	χ^b	$\Delta E^{int\,f}_{bond}$	ΔE_{solv}	$\Delta E^{d,e}_{bond}$
F	18.6	45.9	−77.7	1.20	−13.2	15.4	2.2
Cl	9.1	35.1	−51.6	1.17	−7.4	14.2	6.8
Br	8.6	34.2	−49.0	1.14	−6.2	12.9	6.7
I	6.8	32.1	−43.8	1.13	−5.0	11.6	6.6
NO_2	5.4	28.4	−33.1	0.98	0.7	12.2	12.9
CN	3.7	20.4	−25.9	1.07	−1.8	24.1	22.3

[a] Energy in kcal/mol. [b] $\chi = |\Delta E_{orbital}| /(\Delta E_{dist} + \Delta E_{steric})$. [c] $\Delta E_{steric} = \Delta E_{elstat} + \Delta E_{Pauli}$. [d] $\Delta E_{bond} = \Delta E^{int}_{bond} + \Delta E_{solv}$. [e] Bond energy in solution. [f] Bond energy in the gas phase, see eq 9.

3.1 and 3.2. Thus the most electronegative X has the weakest trans influence, for reasons explained above. We are not aware that such a simple explanation of the "trans influence" has been given before for the series of X ligands discussed here.

3.3. Energy Decomposition Analysis of the Bond between CH_4 and *trans*-$PtCl_2X^-$ in *trans*-$PtCl_2X(CH_4)^-$. Up to now, we have analyzed how different trans ligands X affect the overlap between orbitals on *trans*-$PtCl_2X^-$ and the CH_4 fragment when a methane adduct is formed. We shall now study the interaction between the two fragments in more detail using the extended transition state (ETS) energy decomposition scheme (eq 9).[20–24] The total interaction energy between $PtCl_2X^-$ and CH_4 in the gas phase can be written as

$$\Delta E^{tot}_{bond} = \Delta E_{dist} + [\Delta E_{elstat} + \Delta E_{Pauli}] + \Delta E_{orbital}$$

$$= \Delta E_{dist} + \Delta E_{steric} + \Delta E_{orbital} \quad (9)$$

The first component is referred to as the distortion term ΔE_{dist}, which is the amount of energy taken to promote the two separate fragments, $PtCl_2X^-$ and CH_4, from their equilibrium structures to the structures they will take up in the combined molecule. The second component is the steric repulsion term ΔE_{steric}, which is the sum of ΔE_{elstat} and ΔE_{Pauli} where ΔE_{elstat} is the classical electrostatic interaction between the promoted fragments, and ΔE_{Pauli} represents the repulsive Pauli interaction between occupied orbitals on the two fragments. Finally, the last term, $\Delta E_{orbital}$, stands for the interactions between the occupied molecular orbitals on one fragment and the unoccupied molecular orbitals of the other fragment as well as the mixing of occupied and virtual orbitals within the same fragment (intrafragment polarization). The terms in eq 9 have been evaluated as described elsewhere.[20–22]

Table 5 displays the total interaction energy ΔE^{int}_{bond} in $PtCl_2X(CH_4)^-$ decomposed into the various contributions according to eq 9 for different X. We note that the interaction energy ΔE^{int}_{bond} in absolute terms decreases in the order F > Cl > Br > I > NO_2 > CN as the overlaps between σ_{CH} and $2a_1$ as well as σ^*_{CH} and $1b_1$ decrease for reasons explained previously.

It is not surprising that the system (X = F) with the strongest interaction energy ΔE^{int}_{bond} also has the largest distortion energy, Table 5. Thus a strong interaction ΔE^{int}_{bond} will lead to a considerable donation of charge from σ_{CH} to $2a_1$ as well as a sizable back-donation from $1b_1$ to σ^*_{CH}; see Table 6. Both donation and back-donation will result in an elongation of the C−H bond, Table 7, and an increase in the distortion energy, especially for CH_4.

Table 6. Occupations of Fragment Orbitals in $PtCl_2XCH_4^-$ for Different X (X = F, Cl, Br, I, NO_2, CN)

	occupation			
	Pt fragment		CH_4 fragment	
X	$1b_1$	$2a_1$	σ_{CH}	σ^*_{CH}
F	1.78	0.28	1.70	0.21
Cl	1.89	0.21	1.76	0.09
Br	1.90	0.21	1.77	0.09
I	1.92	0.19	1.79	0.07
NO_2	1.94	0.13	1.83	0.05
CN	1.96	0.09	1.84	0.02

Table 7. Pt−C, Pt−H, and C−H Bond Lengths[a] in *trans*-$PtCl_2X(CH_4)^-$ with Different X (X = F, Cl, Br, I, NO_2, and CN)

	r(Pt−C)	r(Pt−H)	r(C−H)
X	1[b]	2[b]	3[b]
F	2.27	1.63	1.27
Cl	2.36	1.72	1.19
Br	2.38	1.74	1.19
I	2.41	1.77	1.18
NO_2	2.53	1.85	1.15
CN	2.53	1.98	1.13

[a] Bond lengths in Å. [b] See geometry 1 in Scheme 1.

Table 8. Further Decomposition of $\Delta E_{orbital}$ in *trans*-$PtCl_2X(CH_4)^-$ Complexes

	orbital interaction energy ($\Delta E_{orbital}$)[f]					
Pt/C[a]	F	Cl	Br	I	NO_2	CN
All/All[b]	−81.6	−55.2	−52.8	−46.7	−40.2	−36.4
1/2[c]	−48.8	−28.6	−26.9	−23.2	−18.4	−12.6
0/2[d]	−18.1	−9.2	−8.5	−7.0	−5.0	−3.3
1/0[e]	−21.4	−15.9	−15.2	−14.0	−12.2	−8.8

[a] Pt/C means Pt fragment/C (methane) fragment. [b] All/All means all virtual orbitals are kept for both fragments in calculation. [c] 1/2 means one virtual orbital is kept for Pt fragment and two virtual orbitals are kept for CH_4 fragment. [d] 0/2 means no virtual orbitals for Pt fragment but two virtual orbitals are kept for CH_4 fragment. [e] 1/0 means one virtual orbital is kept for Pt fragment and no virtual orbitals for CH_4 fragment. [f] Energy in kcal/mol.

The order of the interaction energy F > Cl > Br > I > NO_2 > CN is also reflected in the steric interaction term ΔE_{steric}. The larger the interaction energy is in absolute terms, the shorter the Pt−C bond length, Table 7, and the larger the steric interaction energy between the two fragments, Table 5. It is important to note that the complex with the strongest Pt−CH_4 bond (X = F) has both the largest destabilizing and (in absolute terms) stabilizing contributions to the total interaction energy ΔE^{int}_{bond}. However, if we consider the ratio

$$\chi = \frac{|\Delta E_{orbital}|}{(\Delta E_{dist} + \Delta E_{steric})} \quad (10)$$

we find that it decreases through the series F > Cl > Br > I > NO_2 > CN. Thus we gain more stabilization per unit of destabilization energy ($\Delta E_{dist} + \Delta E_{steric}$) at the beginning of the series than at the end.

We display finally in Table 8 a further analysis of ΔE_{int} as a function of X. In the first entry "All/All", we have the full interaction energy with all virtual orbitals on the two fragments included. The entry "1/0" stems from a calculation in which $2a_1$ is the only virtual orbital included. The corresponding interaction energy thus represents the stabilization from donation

(20) Ziegler, T.; Rauk, A. *Theor. Chim. Acta* **1977**, *46*, 1.
(21) Ziegler, T.; Rauk, A. *Inorg. Chem.* **1979**, *18*, 1755.
(22) Ziegler, T.; Rauk, A. *Inorg. Chem.* **1979**, *18*, 1558.
(23) Mitoraj, M.; Zhu, H.; Michalak, A.; Ziegler, T. *Organometallics* **2007**, *26*, 1627.
(24) Mitoraj, M.; Zhu, H.; Michalak, A.; Ziegler, T. *J. Org. Chem.* **2006**, *71*, 9208.

Table 9. Decomposition of the Bonding Energy[a,d] between the *trans*-$PtCl_2X^-$ Fragment and H_2O in *trans*-$PtCl_2X(H_2O)^-$ for Different X (X = F, Cl, Br, I, NO_2, and CN)

X	ΔE_{dist}	ΔE^c_{steric}	$\Delta E_{orbital}$	χ^b	$\Delta E^{int\,f}_{bond}$	ΔE_{solv}	$\Delta E^{d,e}_{bond}$
F	4.5	16.9	−43.1	2.02	−21.7	9.3	−12.4
Cl	1.6	16.9	−36.1	1.95	−17.6	9.3	−8.3
Br	1.6	17.9	−35.8	1.84	−16.3	8.2	−8.1
I	1.1	18.9	−35.0	1.74	−15.0	7.4	−7.6
NO_2	4.2	18.9	−33.1	1.43	−10.0	3.3	−6.7
CN	1.4	12.7	−28.0	1.99	−14.0	15.6	1.6

[a] Energy in kcal/mol. [b] $\chi = |\Delta E_{orbital}| / (\Delta E_{dist} + \Delta E_{steric})$. [c] $\Delta E_{steric} = \Delta E_{elstat} + \Delta E_{Pauli}$. [d] $\Delta E_{bond} = \Delta E^{int}_{bond} + \Delta E_{solv}$. [e] Bond energy in solution. [f] Bond energy in the gas phase, see eq 9.

into $2a_1$. In the same way, the entry "0/2" represents the stabilization due to donation into σ^*_{CH}. Finally, 1/2 has both donations to $2a_1$ as well as σ^*_{CH}. We note that the interaction energy for 1/2 in absolute terms exceeds the sum of 1/0 + 0/2, thus testifying to some synergism. On the other hand 1/0 + 0/2 is much smaller than All/All in absolute terms. The difference represents intrafragment polarizations to compensate for the steric interaction energy ΔE_{steric}.

In order to obtain the total bond strength ΔE_{bond}, we have to add to the gas-phase bond energy ΔE^{int}_{bond} the contribution from the solvation energy ΔE_{solv}. The change in solvation energy ΔE_{solv} from $PtCl_2X^- + CH_4$ to $PtCl_2X(CH_4)^-$ is positive, as $PtCl_2X(CH_4)^-$ has a larger volume than $PtCl_2X^-$. After the inclusion of solvation effects, the order of the "trans influence" is F < Cl ∼ Br ∼ I < NO_2 < CN in $PtCl_2X(CH_4)^-$.

3.4. Energy Decomposition Analysis of Bond between H_2O and *trans*-$PtCl_2X^-$ in *trans*-$PtCl_2X(H_2O)^-$. The most favorable pathway of methane uptake for *trans*-$PtCl_2X(H_2O)^-$ is the substitution of H_2O by CH_4, and its energy barrier is largely determined by the dissociation energy of H_2O, as demonstrated in a previous investigation.[3] The energy decomposition of the bond between H_2O and *trans*-$PtCl_2X^-$ in $PtCl_2X(H_2O)^-$ is shown in Table 9.

The bonding energy in *trans*-$PtCl_2X(H_2O)^-$ between *trans*-$PtCl_2X^-$ and H_2O decreases in the order F > Cl > Br > I > NO_2 > CN, see ΔE^{int}_{bond}, which is in accordance with the prediction by the trans-directing ability of the trans ligand X. The above trend is reflected in χ, the increase of $|\Delta E_{orbital}|$ per unit energy of $(\Delta E_{dist} + \Delta E_{steric})$, as χ is largest for F and smallest for NO_2. Behind this trend is the reduction in the overlap between the *trans*-$PtCl_2X^-$ and the H_2O fragments, as X becomes less electronegative just as in the interaction between *trans*-$PtCl_2X^-$ and CH_4; see Sections 3.1 and 3.2. Solvation energy does not alter the trend in ΔE_{bond}, which is determined by electronic effects.

3.5. Energy Decomposition Analysis of Interaction between CH_4 and $PtCl_2X^-$ in C−H Activation Transition State 3. After the formation of the methane complex $PtCl_2X(CH_4)^-$, the system might proceed with the C−H activation through the transition state 3 of Scheme 1. We note that we were unable to find a transition state for X = F. In this case, $PtCl_2F(CH_4)^-$ proceeds directly to the C−H activation product without an energy barrier.

Table 10 displays key geometrical parameters of the transition state for C−H activation of CH_4 by *trans*-$PtCl_2X^-$; see complex 3 of Scheme 1. It is clearly seen that the C−H bond is lengthened while the Pt−C and Pt−H bonds are shortened, compared to the $PtCl_2X(CH_4)^-$ complex 1 of Scheme 1. The geometry of 3 is very similar for different X. Thus, the bond lengths are the same to within 0.22 Å for Pt−C, 0.04 Å for Pt−H, and 0.11 Å for the C−H bond. The similar structure of CH_4 in 3 is also reflected in the modest variation in ΔE_{dist}, Table 11.

Table 10. Bond Lengths[a] in Transition State for C−H Activation of CH_4 by $PtCl_2X^-$ with Different X (X = F, Cl, Br, I, NO_2, and CN)

X	*r*(Pt−C) 1[b]	*r*(Pt−H) 2[b]	*r*(C−H) 3[b]
F			
Cl	2.14	1.59	1.36
Br	2.13	1.60	1.34
I	2.05	1.63	1.25
NO_2	1.93	1.63	1.27
CN	2.15	1.61	1.31

[a] Bond lengths in Å. [b] See geometry 3 in Scheme 1.

Table 11. Decomposition of the Bonding Energy[a,d] between the *trans*-$PtCl_2X^-$ Fragment and the CH_4 Fragment in *trans*-$PtCl_2X(CH_4)^-$ for Different X (X = F, Cl, Br, I, NO_2, and CN) at the Transition State

X	ΔE_{dist}	ΔE^c_{steric}	$\Delta E_{orbital}$	χ^b	$\Delta E^{int\,f}_{bond}$	ΔE_{solv}	$\Delta E^{d,e}_{bond}$
F							
Cl	29.7	60.2	−91.5	1.02	−1.6	13.6	12.0
Br	34.2	64.6	−96.5	0.98	2.3	12.6	14.9
I	30.8	66.9	−96.6	0.99	1.1	11.6	12.7
NO_2	28.8	86.5	−98.5	0.85	16.8	10.8	27.6
CN	33.2	105.8	−111.7	0.80	27.3	25.9	53.2

[a] Energy in kcal/mol. [b] $\chi = |\Delta E_{orbital}| / (\Delta E_{dist} + \Delta E_{steric})$. [c] $\Delta E_{steric} = \Delta E_{elstat} + \Delta E_{Pauli}$. [d] $\Delta E_{bond} = \Delta E^{int}_{bond} + \Delta E_{solv}$. [e] Bond energy in solution. [f] Bond energy in the gas phase, see eq 9.

Scheme 1. Structures of *trans*-$PtCl_2X(CH_4)^-$ at Reactant (1) and Transition State (3) and of *trans*-$PtClX_2(CH_4)^-$ at Reactant (2) and Transition State (4)

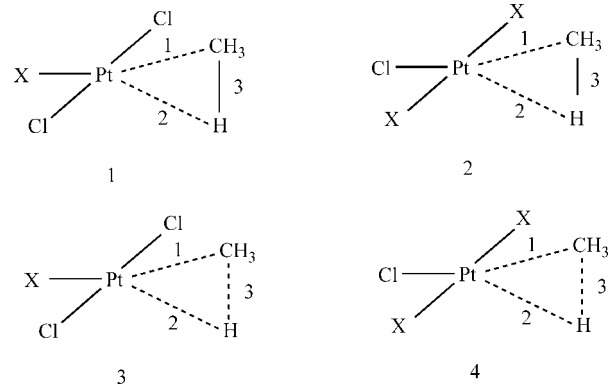

Table 11 displays the interaction energy ΔE^{int}_{bond} decomposed according to eq 9 for the transition state 3. We note that ΔE^{int}_{bond} becomes increasingly positive and destabilizing through the series Cl < Br < I < NO_2 < CN. This trend is set by the ratio χ defined in eq 10. Thus the amount of stabilizing orbital interaction obtained in absolute terms per unit of steric interaction and distortion is largest at the start of the series, as the overlaps here are larger between $2a_1$ and σ_{CH} as well as $1b_1$ and σ^*_{CH}; see Table 4. The term ΔE_{bond} exhibits the same trend, but the inclusion of solvation energy enlarges the energy gap between the halogen ligands and NO_2 and CN.

3.6. Energy Decomposition Analysis of the Bond between *trans*-$PtClX_2^-$ and CH_4 in *trans*-$PtClX_2(CH_4)^-$ at the Reactant and Transition State. After having analyzed how the trans ligand X affects the C−H activation of *trans*-$PtCl_2X(CH_4)^-$, we now turn to the influence of the cis ligand X on C−H activation, taking as our example the *trans*-$PtClX_2(CH_4)^-$, complex 2 of Scheme 1.

Table 12 displays the energy decomposition of the bond between *trans*-$PtClX_2^-$ and CH_4 in *trans*-$PtClX_2(CH_4)^-$. In

Table 12. Decomposition of the Bonding Energy[a,d] between the *trans*-$PtClX_2^-$ Fragment and CH_4 in *trans*-$PtClX_2(CH_4)^-$ for Different X (X = F, Cl, Br, I, NO_2 and CN)

X	ΔE_{dist}	ΔE^c_{steric}	$\Delta E_{orbital}$	χ^b	$\Delta E^{int}{}^f_{bond}$	ΔE_{solv}	$\Delta E^{d,e}_{bond}$
F	10.1	32.7	−52.9	1.24	−10.1	17.9	7.8
Cl	9.1	35.1	−51.6	1.17	−7.4	14.2	6.8
Br	10.0	35.2	−52.7	1.17	−7.5	11.5	4.0
I	10.3	37.6	−56.2	1.17	−8.3	8.8	0.5
NO_2	20.6	28.0	−47.9	0.98	0.7	4.1	4.8
CN	7.7	27.9	−48.1	1.35	−12.5	7.5	−5.0

[a] Energy in kcal/mol. [b] $\chi = |\Delta E_{orbital}| / (\Delta E_{dist} + \Delta E_{steric})$. [c] $\Delta E_{steric} = \Delta E_{elstat} + \Delta E_{Pauli}$. [d] $\Delta E_{bond} = \Delta E^{int}{}_{bond} + \Delta E_{solv}$. [e] Bond energy in solution. [f] Bond energy in the gas phase, see eq 9.

Table 13. Decomposition of the Bonding Energy[a,d] between the *trans*-$PtClX_2^-$ Fragment and the CH_4 Fragment in *trans*-$PtClX_2(CH_4)^-$ for Different X (X = F, Cl, Br, I, NO_2, and CN) at the Transition State

X	ΔE_{dist}	ΔE^c_{steric}	$\Delta E_{orbital}$	χ^b	$\Delta E^{int}{}^f_{bond}$	ΔE_{solv}	$\Delta E^{d,e}_{bond}$
F	22.9	50.2	−80.8	1.11	−7.7	17.4	9.7
Cl	26.2	60.2	−91.5	1.06	−5.1	13.6	8.5
Br	28.9	60.6	−94.9	1.06	−5.4	11.1	5.7
I	24.8	58.9	−90.4	1.08	−6.7	8.2	1.5
NO_2	31.2	51.7	−79.4	0.96	3.5	3.3	6.8
CN	27.2	61.8	−96.7	1.09	−7.7	7.8	0.1

[a] Energy in kcal/mol. [b] $\chi = |\Delta E_{orbital}| / (\Delta E_{dist} + \Delta E_{steric})$. [c] $\Delta E_{steric} = \Delta E_{elstat} + \Delta E_{Pauli}$. [d] $\Delta E_{bond} = \Delta E^{int}{}_{bond} + \Delta E_{solv}$. [e] Bond energy in solution. [f] Bond energy in the gas phase, see eq 9.

Table 14. Decomposition of the Energy Barrier[a] of C−H Activation of *trans*-$PtCl_2X(CH_4)^-$ for Different X (X = F, Cl, Br, I, NO_2, and CN)

X	$\Delta E^{\ddagger}{}_{dist}{}^b$	$\Delta E^{\ddagger}{}_{steric}{}^{c,h}$	$\Delta E^{\ddagger}{}_{orbital}{}^d$	$\chi^{\ddagger}{}_e$	$\Delta E^{\ddagger}{}_g{}^i$	$\Delta E^{\ddagger}{}_{solv}{}^f$	$\Delta E^{\ddagger}{}_s{}^j$
F							
Cl	20.6	25.2	−40.0	0.87	5.8	−0.7	5.1
Br	25.6	30.4	−47.5	0.85	8.5	−0.3	8.2
I	24.0	34.9	−52.8	0.90	6.1	0.0	6.1
NO_2	23.4	58.1	−65.3	0.80	16.2	−1.4	14.8
CN	29.5	85.4	−85.8	0.75	29.1	1.8	30.9

[a] Energy in kcal/mol. [b] $\Delta E^{\ddagger}_{dist} = \Delta E^{TS}_{dist} - \Delta E^{G}_{dist}$. [c] $\Delta E^{\ddagger}_{steric} = \Delta E^{TS}_{steric} - \Delta E^{G}_{steric}$. [d] $\Delta E^{\ddagger}_{orbital} = \Delta E^{TS}_{orbital} - \Delta E^{G}_{orbital}$. [e] $\chi^{\ddagger} = |\Delta E^{\ddagger}_{orbital}| / (\Delta E^{\ddagger}_{dist} + \Delta E^{\ddagger}_{steric})$. [f] $\Delta E^{\ddagger}_{solv} = \Delta E^{TS}_{solv} - \Delta E^{G}_{solv}$. [h] $\Delta E_{steric} = \Delta E_{elstat} + \Delta E_{Pauli}$. [i] $\Delta E^{\ddagger}_g = \Delta E^{int,TS}_{bond} - \Delta E^{int,G}_{bond}$, see eq 9 for $\Delta E^{int}{}_{bond}$. [j] $\Delta E^{\ddagger}_s = \Delta E^{TS}{}_{bond} - \Delta E^{G}{}_{bond}$ in solution, $\Delta E_{bond} = \Delta E^{int}{}_{bond} + \Delta E_{solv}$.

considering ΔE_{bond} of Table 12, we note that the stability of the Pt−CH_4 bond in solution follows the order F < Cl < Br < NO_2 < I < CN, which, except for the relative position of NO_2, I, is the opposite of that of the trans influence in $PtCl_2X(CH_4)^-$. The trend is set by the solvation energies ΔE_{solv}, which follows the trend F > Cl > Br > NO_2 > I > CN. For the majority of the systems ΔE_{solv} is positive, as the product *trans*-$PtX_2Cl(CH_4)^-$ has a larger volume, and consequently less solvation stabilization, than the reactant *trans*-PtX_2Cl^-. The change in volume is largest at the start of the series.

For the transition state 4 in Scheme 1, ΔE_{bond} of Table 13 follows the same trend as in the adduct $PtX_2Cl(CH_4)^-$. The trend is again set by ΔE_{solv}. It is perhaps not so surprising that electronic factors have only a modest influence on the trend in the Pt−CH_4 bond strength as a function of X both in the adduct $PtX_2Cl(CH_4)^-$ 2 and the transition state 4 since all systems have the same ligand trans to the Pt−CH_4 bond.

3.7. Comparison of the C−H Cleavage Energy Barrier of *trans*-$PtCl_2X(CH_4)^-$ and *trans*-$PtClX_2(CH_4)^-$. Tables 14 and 15 display the energy barriers $\Delta E^{\ddagger}$ both in the gas phase and in solution for C−H cleavage involving *trans*-$PtCl_2X(CH_4)^-$ and *trans*-$PtClX_2(CH_4)^-$, respectively. $\Delta E^{\ddagger}$ is further decomposed into its activation components $\Delta E^{\ddagger}_{dist}$, $\Delta E^{\ddagger}_{steric}$, $\Delta E^{\ddagger}_{orbital}$, and $\Delta E^{\ddagger}_{solv}$. Here $\Delta E^{\ddagger}_{dist} = \Delta E^{TS}_{dist} - \Delta E^{G}_{dist}$ with similar definitions for the other components; see Tables 14 and 15. The term $\chi^{\ddagger}$, the increase in $\Delta E^{\ddagger}_{orbital}$ as per unit energy of $\Delta E^{\ddagger}_{dist}$ and $\Delta E^{\ddagger}_{steric}$, is also calculated for both Pt species.

Table 15. Decomposition of the Energy Barrier[a] of C−H Activation of *trans*-$PtClX_2(CH_4)^-$ for Different X (X = F, Cl, Br, I, NO_2, and CN)

X	$\Delta E^{\ddagger}{}_{dist}{}^b$	$\Delta E^{\ddagger}{}_{steric}{}^{c,h}$	$\Delta E^{\ddagger}{}_{orbital}{}^d$	$\chi^{\ddagger}{}_e$	$\Delta E^{\ddagger}{}_g{}^i$	$\Delta E^{\ddagger}{}_{solv}{}^f$	$\Delta E^{\ddagger}{}_s{}^j$
F	12.8	17.5	−28.0	0.92	2.3	−0.5	1.8
Cl	17.2	25.2	−40.0	0.94	2.4	−0.7	1.7
Br	18.9	25.5	−42.2	0.95	2.2	−0.4	1.8
I	14.5	21.3	−34.2	0.95	1.6	−0.6	1.0
NO_2	10.6	23.7	−31.6	0.92	2.7	−0.9	1.8
CN	19.5	34.8	−48.6	0.90	5.7	0.3	6.0

[a] Energy in kcal/mol. [b] $\Delta E^{\ddagger}_{dist} = \Delta E^{TS}_{dist} - \Delta E^{G}_{dist}$. [c] $\Delta E^{\ddagger}_{steric} = \Delta E^{TS}_{steric} - \Delta E^{G}_{steric}$. [d] $\Delta E^{\ddagger}_{orbital} = \Delta E^{TS}_{orbital} - \Delta E^{G}_{orbital}$. [e] $\chi^{\ddagger} = |\Delta E^{\ddagger}_{orbital}| / (\Delta E^{\ddagger}_{dist} + \Delta E^{\ddagger}_{steric})$. [f] $\Delta E^{\ddagger}_{solv} = \Delta E^{TS}_{solv} - \Delta E^{G}_{solv}$. [h] $\Delta E_{steric} = \Delta E_{elstat} + \Delta E_{Pauli}$. [i] $\Delta E^{\ddagger}_g = \Delta E^{int,TS}_{bond} - \Delta E^{int,G}_{bond}$, see eq 9 for $\Delta E^{int}{}_{bond}$. [j] $\Delta E^{\ddagger}_s = \Delta E^{TS}{}_{bond} - \Delta E^{G}{}_{bond}$ in solution, $\Delta E_{bond} = \Delta E^{int}{}_{bond} + \Delta E_{solv}$.

It is clearly seen from Table 14 that the energy barrier for C−H activation in the case of *trans*-$PtCl_2X(CH_4)^-$ increases in the order Cl ∼ Br ∼ I < NO_2 < CN both in the gas phase and in solution. Among the different components, $\Delta E^{\ddagger}_{dist}$ varies modestly among Cl, Br, I, and NO_2, but increases substantially for X = CN. This is understandable since CH_4 for X = CN is only modestly distorted in the ground state of $PtCl_2X(CH_4)^-$. It must then undergo the largest distortion to reach the transition state where CH_4 is equally distorted for all systems. Both $\Delta E^{\ddagger}_{steric}$ and $\Delta E^{\ddagger}_{orbital}$ increase continuously in absolute terms from Cl to CN.

We can understand this trend by observing that the system with the strongest trans-directing ligand has the longest Pt−CH_4 distance in the ground state, whereas the Pt−CH_4 distances are quite similar for all systems in the transition state. Thus the system with the most trans-directing ligand must undergo the largest change in the Pt−CH_4 bond length and consequently the largest variation in $\Delta E^{\ddagger}_{steric}$ and $\Delta E^{\ddagger}_{orbital}$. It is finally worth noting that the activation correlates with $\chi^{\ddagger}$, the stabilization gained in $-\Delta E^{\ddagger}_{orbital}$ for each energy unit spent of $\Delta E^{\ddagger}_{steric} + \Delta E^{\ddagger}_{dist}$, Table 14. The systems with the larger $\chi^{\ddagger}$ are those with the lower barrier and the higher overlap of $\langle \sigma_{CH} | 2a_1 \rangle$ and $\langle \sigma^*_{CH} | 1b_1 \rangle$.

Table 15 exhibits the energy barrier and its components for C−H activation in the case of *trans*-$PtClX_2(CH_4)^-$. Due to the similarities in geometry of the Pt−CH_4 frame in *trans*-$PtClX_2(CH_4)^-$, both at the ground state and the transition state with different X, $\Delta E^{\ddagger}_{steric}$, $\Delta E^{\ddagger}_{dist}$, and $\Delta E^{\ddagger}_{orbital}$ vary only slightly from F to CN. Also $\Delta E^{\ddagger}_{solv}$ is modest as the solvation energy changes little from adduct to transition state. However, a jump in $\Delta E^{\ddagger}$ is seen for X = CN.

4. Conclusion

We have studied the influence of different ligands X (X = F, Cl, Br, I, NO_2, CN) on the Pt−CH_4 bond and C−H activation barriers in *trans*-$PtCl_2X(CH_4)^-$, **1**, and *trans*-$PtX_2Cl(CH_4)^-$, **2**, where X is respectively trans (**1**) and cis (**2**) to CH_4. For **1** with X trans to CH_4, we find that the Pt−CH_4 bond energy decreases as F > Cl > Br > I > NO_2 > CN, in agreement with the experimentally established "trans influence" of these ligands.

The Pt−CH_4 bond in complex 1 of Scheme 1 is established through the bonding interaction between the empty $2a_1$ σ orbital on *trans*-$PtCl_2X^-$ and σ_{CH} on CH_4 as well as between the occupied $1b_1$ orbital on the metal fragment and σ^*_{CH} on CH_4. Here $2a_1$ is an out-of-phase combination between d_σ on the metal

and σ_x on X. Likewise, $1b_1$ is an out-of-phase combination between d_π on Pt and π_x on the ligand X. Through the series X = F, Cl, Br, I, NO_2, CN, the orbital energies of σ_x and π_x increase due to the decrease of the electronegativity of the elements involved in the orbitals. As a result, the contribution to $2a_1$ and $1b_1$ increases, whereas the d contribution declines. The decline in d- contribution will in turn lead to a decrease in the bonding overlaps $\langle \sigma_{CH} | 2a_1 \rangle$ and $\langle \sigma^*_{CH} | 1b_1 \rangle$, as only the d component in $2a_1$ and $1b_1$ contributes to these overlaps. The decline in the bonding overlaps will in turn weaken the Pt−CH_4 bond. Thus the experimentally well-established "trans influence" for the series of ligands investigated here can be related to their electronegativity. The trans effect is even more pronounced in the transition state with the result that the barrier of C−H activation with CH_4 trans to X follows the order F < Cl < Br < I < NO_2 < CN.

When X is situated in the cis position, the stability of *trans*-$PtX_2Cl(CH_4)^-$ in both the ground state and transition state follows the order F < Cl < Br < NO_2 < I < CN. The order is set by solvent effects that favor the association process

$$\textit{trans}\text{-}PtX_2Cl^- + CH_4 \rightarrow \textit{trans}\text{-}PtX_2Cl(CH_4)^-$$

for ligands X with a large volume.

Not only C−H activation, but also the rate-determining methane uptake step is influenced by the trans ligand. There are many reports on ligand displacement rather than C−H bond cleavage as the rate-determining step with various metal centers, including Pt.[25–27] As one might expect from our analysis, they all involve weakly trans-directing ligands. However, as the trans-directing ability of X increases, the uptake barrier decreases as the Pt−L bond for the leaving group L is weakened, whereas the C−H activation barrier increases. This trend was illustrated by calculations on $PtCl_2X(H_2O)^-$; see Table 16. It is thus clear that the optimal trans ligand X in the Shilov systems is one that labilizes the leaving ligand sufficiently without causing a substantial C−H activation barrier.

Table 16. Comparison of the Activation Energy of Methane Uptake and C−H Activation with Different Trans Ligand in *trans*-$PtCl_2X(H_2O)^-$

	activation energy ($\Delta G^{\ddagger}_s$)[a]	
ligand	methane uptake[b]	C−H activation[b]
F	31.3	0
Cl	23.3	1.1
Br	23.4	2.1
I	22.0	3.6
NO_2	20.9	16.6
CN	24.9	28.6

[a] Energy in kcal/mol. [b] Data are from ref 5.

Acknowledgment. This work was supported by NSERC. T.Z. would to thank the Canadian government for a Canada Research Chair.

OM701149F

(25) Jones, W. D. *Inorg. Chem.* **2005**, *44*, 4475.
(26) Labinger, J. A.; Bercaw, J. E. *Nature* **2002**, *417*, 507.
(27) Lersch, M.; Tilset, M. *Chem. Rev.* **2005**, *105*, 2471.